IEEE Access
Multidisciplinary ⋮ Rapid Review ⋮ Open Access Journal

Received 23 January 2023, accepted 7 February 2023, date of publication 13 February 2023, date of current version 23 February 2023.

Digital Object Identifier 10.1109/ACCESS.2023.3244190

RESEARCH ARTICLE

Improved Super-Twisting Non-Singular Fast Terminal Sliding Mode Control of Interior Permanent Magnet Synchronous Motor Considering Time-Varying Disturbance of the System

XIANGFEI LI, JUNQIN LIU, YANG YIN, AND KAIHUI ZHAO, (Senior Member, IEEE)
College of Electrical and Information Engineering, Hunan University of Technology, Zhuzhou 412007, China

Corresponding author: Xiangfei Li (lixiangfei2006@163.com)

This work was supported in part by the National Key Research and Development Program of China under Grant 2021YFF0501100, in part by the Natural Science Foundation of China under Grant 61473117 and Grant 62173137, in part by the Scientific Research Fund of the Hunan Provincial Education Department under Grant 18A267, and in part by the Key Laboratory for Electric Drive Control and Intelligent Equipment of Hunan Province under Grant 2016TP1018.

ABSTRACT To solve the problems that control performance of high torque traction interior permanent magnet synchronous motor (IPMSM) is degraded by parameter perturbation and unknown disturbance, this paper proposes a novel Improved Super-Twisting non-singular fast terminal sliding mode control strategy (IST-NFTSMC) for IPMSM based on Extended Nonsingular Fast Terminal Sliding Mode Disturbance Observer (ENFTSMDO). Firstly, the mathematical model of IPMSM under parameter perturbation is established; Then, an improved Super-Twisting nonsingular fast terminal sliding mode speed controller (IST-NFTSMC) based on extended nonsingular fast terminal sliding mode disturbance observer (ENFTSMDO) is designed, in which the improved Super-Twisting control law designed can effectively weaken the chattering of traditional NFTSMC, and ENFTSMDO can more accurately observe the unknown disturbance part of the system in real-time than ESMDO; Finally, compared with PI control and traditional NFTSMC control by simulations and experiments, the method proposed has merits of accelerating convergence, improving steady-state accuracy and minimizing the current and torque pulsation.

INDEX TERMS Interior permanent magnet synchronous motor (IPMSM), improved super twisting (IST-), nonsingular fast terminal sliding mode (NFTSM), extended nonsingular fast terminal sliding mode disturbance observer (ENFTSMDO).

I. INTRODUCTION

Interior permanent magnet synchronous motor (IPMSM) has been widely used in Urban rail transit, intelligent robots, and other related fields because of its Strong overload capacity, small size, and other advantages [1], [2], [3]. Compared with the asynchronous motor, the IPMSM has lower torque ripple and higher average efficiency in the speed control system [4]. At present, PI control is widely used in the field of train traction engineering due to its simple algorithm and mature technology [5]. However, IPMSM is vulnerable to unknown disturbances and other uncertain factors. But the traditional linear PI control can't suppress the influence of disturbances due to its integral saturation and other limitations, resulting in the overall control performance degradation [6]. For the high-performance control of IPMSM in speed regulation systems, many advanced control methods have been applied to the field of motor control, such as inverse control [7], robust control [8], state feedback control [9], adaptive control [10], sliding mode control (SMC) [11], [12], [13], [14],

The associate editor coordinating the review of this manuscript and approving it for publication was Kan Liu.

etc. Among them, the SMC algorithm has attracted much attention because of its simple algorithm and strong external anti-interference [15].

Because SMC can change the dynamic characteristics of the drive system by using the switching control law, it is insensitive to the changes in system parameters and can maintain a fast dynamic response [16]. Compared with traditional Line Sliding Mode Control (LSM), it has the characteristics of gradual convergence [17], Terminal Sliding Mode (TSM) can achieve finite time convergence, but it will make the system singular [18]; Integrated Sliding Mode Control (ISM) can accelerate the convergence speed, but the chattering is large [19]; NFTSM eliminates the singularity of TSM and realizes the rapid convergence of the controlled system in a finite time [19]. In [8], a finite set model fault-tolerant predictive control algorithm is proposed, which effectively suppressed the system disturbance, but the system tracking accuracy needs to be improved. According to the traditional sliding mode theory, an improved NTSMC method is proposed, which combines MFC and NTSM, but only considers fault tolerant control in the case of loss of excitation, without considering the impact of other motor parameter changes on the system [20]. In [21], an adaptive NTSM flux observer is designed to accurately estimate flux. [22] uses the traditional sliding mode observer (SMO) to estimate the unknown part of the super local model, and feedforward compensation can effectively suppress parameter perturbation, but the chattering caused by the high gain of the traditional SMO cannot be avoided. Compared with [22], [23] proposes a new super 64 local model and uses an ESMDO to estimate the unknown part of the super local model, effectively suppressing the 66 current ripple under parameter perturbation, and improving the robustness of the control system. [24] proposes a deadbeat predictive control algorithm based on the combination of a new reaching law and an extended state observer (ESO), which effectively increases the robustness of the system while ensuring the current rapidity. In [25], an intelligent super twisting sliding mode controller is designed for the robust control of power flow between the motor stator and the power grid of the wind turbine generator, the simulation demonstrates that the method can effectively eliminate the power fluctuation in traditional methods. [26] uses a super-twisting sliding mode control method to track and control the output speed of switched reluctance motor, effectively eliminating chattering. In [28], a super-twisting sliding mode observer 80 based on model reference adaptive is designed for ship six-phase induction motor.

In order to improve the control performance of IPMSM under time-varying disturbances, this paper proposes an improved super-twisting non-singular fast terminal sliding mode control method (IST-NFTSMC) for IPMSM based on the extended non-singular fast terminal sliding mode disturbance observer (ENFTSMDO). This method combines the third-order super-twisting (IST-) and nonsingular fast terminal sliding mode (NFTSM) to form an improved nonsingular fast terminal sliding mode controller, while designing an extended non-singular fast terminal sliding mode disturbance observer to accurately estimate the unknown partial disturbance in real time and feedforward compensation for IST-NFTSMC. The anti-interference ability and robustness of the motor closed-loop control system are effectively improved, and the fault-tolerant control of IPMSM under parameter perturbation and unknown disturbance is realized. Finally, simulation and RT-Lab experimental results verify the effectiveness of the proposed control algorithm.

II. MATHEMATICAL MODEL OF IPMSM

Ignoring stator core saturation, parameter perturbation, and hysteresis loss [4], the stator voltage equation of IPMSM in the d-q axis coordinate can be expressed as:

$$\begin{cases} u_d = R_s i_d + L_d \dfrac{di_d}{dt} - \omega_e L_q i_q \\ u_q = R_s i_q + L_q \dfrac{di_q}{dt} + \omega_e \left(L_d i_d + \psi_f\right) \end{cases} \tag{1}$$

where L_d, L_q are the d-q axis inductances (H); i_d, i_q are the d-q axis stator currents (A); u_d, u_q are the d-q axis stator voltages (V); R_s is stator resistance (Ω); ψ_f is permanent magnet flux linkage (Wb); ω_e is the electric angular velocity (rad/s).

During the actual operation of IPMSM, the internal parameters of the motor will be perturbed due to temperature, mechanical stress, and other factors. Considering the influence of electromagnetic parameter perturbation, the IPMSM mathematical model can be expressed as [22]:

$$\begin{cases} u_d = R_s i_d + L_d \dfrac{di_d}{dt} - \omega_e L_q i_q + \Delta u_d \\ u_q = R_s i_q + L_q \dfrac{di_q}{dt} + \omega_e (L_d i_d + \psi_f) + \Delta u_q \end{cases} \tag{2}$$

where Δu_d, Δu_q are the d-q axis voltage disturbances caused by parameter perturbation, respectively.

The electromagnetic torque equation of IPMSM can be expressed as:

$$T_e = \frac{3}{2} n_p \left[\psi_f + \left(L_d - L_q\right) i_d\right] i_q = \frac{3}{2} n_p \psi_{ext} i_q \tag{3}$$

where T_e is the electromagnetic torque (N · m); $\psi_{ext} = \psi_f + \left(L_d - L_q\right) i_d$ is the effective flux; n_p is the pole number (pairs).

Considering the influence of electromagnetic parameter perturbation, the electromagnetic torque equation of IPMSM can be expressed as:

$$T_e = \frac{3}{2} n_p \psi_{ext} i_q + \Delta T_e \tag{4}$$

where ΔT_e is the electromagnetic torque by parameter perturbation.

The mechanical motion equation of IPMSM can be expressed as:

$$\frac{d\omega_e}{dt} = \frac{n_p}{J} \left(T_e - T_L - B\omega_m\right) \tag{5}$$

where T_L is the load torque (N·m); J is the moment of inertia (Kg · m^2); B is the damping coefficient (N · m · s); ω_m is the mechanical angular speed of the motor (rad/s).

Considering the influence of electromagnetic parameter perturbation, the mechanical motion equation of IPMSM can be expressed as:

$$\frac{d\omega_e}{dt} = \frac{n_p}{J}(T_e - T_L - B\omega_m) + \Delta P_n \tag{6}$$

where ΔP_n is the disturbance caused by the change of B and J.

Substitute Eq. (5) into Eq. (6)

$$\begin{aligned}\frac{d\omega_e}{dt} &= \frac{3n_p^2}{2J}\psi_{ext} i_q - \frac{B}{J}\omega_e - \frac{n_p}{J}(\Delta T_e - T_L + \Delta T_L) + \Delta P_n \\ &= \gamma i_q + \xi\omega_e + F\end{aligned} \tag{7}$$

where γ and ξ are parameters to be designed; $\xi = B/J$; $\gamma = 3n_p^2\psi_{ext}/2J$; F is the known part and unknown disturbance part of the system.

III. DESIGN OF IST-NFTSMC CONTROLLER BASED ON ENFTSMDO

Considering the influence of parameter perturbation and unknown disturbances, to achieve high-performance control of the IPMSM, accelerate the speed transient response, and improve the steady-state control accuracy, In this section, combining improved Super-Twisting with NFTSMC, an IST-NFTSMC speed controller is designed. It can effectively reduce chattering and achieve rapid convergence.

A. DESIGN OF IST-NFTSMC CONTROL

From Eq. (7), the control law of the speed controller can be designed as follows [22]:

$$i_q^* = \frac{\dot{\omega}_e^* - \xi\omega_e - F + u_c}{\gamma} \tag{8}$$

where i_q^* is the given value of the q-axis current component; ω_e^* is the given speed of the system; u_c is the feedback output control law of IST-NFTSMC.

Substitute Eq. (7) into Eq. (8)

$$\dot{\omega}_e^* - \dot{\omega}_e + u_c = 0 \tag{9}$$

Define the error between the given speed value and the actual value as follows:

$$e = \omega_e^* - \omega_e \tag{10}$$

The equation of state is designed as follows:

$$\begin{cases}\dot{e}_1 = e_2 \\ \dot{e}_2 = \dot{e}\end{cases} \tag{11}$$

To effectively accelerate the speed error convergence rate, the nonsingular fast terminal sliding surface (NFTSM) is designed as follows [19]:

$$s = e_1 + \alpha e_1^{g/h} + \beta e_2^{p/q} \tag{12}$$

where $\alpha > 0$; $\beta > 0$; g, h, p and q are odd numbers to be designed; $1 < p/q < 2$; $g/h > p/q$.

Taking the derivative of Eq. (12)

$$\begin{aligned}\dot{s} &= \dot{e}_1 + \alpha\frac{g}{h}e_1^{g/h-1}e_2 + \beta\frac{p}{q}e_2^{p/q-1}\dot{e}_2 \\ &= e_2 + \alpha\frac{g}{h}e_1^{g/h-1}e_2 + \beta\frac{p}{q}e_2^{p/q-1}\dot{e}_2\end{aligned} \tag{13}$$

When $s = 0$, the following equation is obtained:

$$\begin{aligned}e_2 &= -(\beta^{-1}(e_1 + \alpha e_1^{g/h}))^{q/p} \\ &= \upsilon(e_1 + \alpha e_1^{g/h}))^{q/p}\end{aligned} \tag{14}$$

where $\upsilon = -\beta^{-q/p}$; $\upsilon < 0$.

To enable the state variables of the control system to enter the sliding mode, the third-order Super-Twisting controlling law is introduced as follows [27]:

$$\begin{cases}\dot{s} = -k_1|s|^{\frac{1}{2}}\,\mathrm{sgn}(s) + k_2 s + g \\ \dot{g} = -k_3\mathrm{sgn}(s) + \dot{F}\end{cases} \tag{15}$$

where $k_1 > 0$; $k_2 < 0$; $k_3 > 0$.

Theorem 1: For Eq. (10), Eq. (12), and Eq. (15) are selected, the IST-NFTSMC feedback control law as shown in Eq. (16) is designed

$$\begin{aligned}u_c = &\frac{q}{\beta p}e_2^{2-p/q}\cdot\left(1 + \frac{\alpha g}{h}e_1^{g/h-1}\right) + k_1|s|^{1/2}\mathrm{sgn}(s) \\ &-k_2 s + \int(k_3\mathrm{sgn}(s) + \dot{F})dt\end{aligned} \tag{16}$$

If Eq. (15) satisfies the condition of Eq. (17), the state error e will converge in finite time.

$$\begin{cases}k_1^2 + 2k_3 + 2\dot{F}\mathrm{sgn}(s) > 0 \\ 5k_2^2(k_1^2 + 2k_3 + 2\dot{F}\mathrm{sgn}(s)) > 0 \\ k_2^2(9k_1^2 + 8k_3 + 28\dot{F}\mathrm{sgn}(s) + 20\dot{F}^2/k_1^2) < 0\end{cases} \tag{17}$$

Proof 1: The following Lyapunov function V is selected as:

$$V = \frac{1}{2}e_1^2 \tag{18}$$

Take the derivative of V:

$$\begin{aligned}\dot{V} &= e_1\dot{e}_1 \\ &= e_1\cdot\upsilon(e_1 + \alpha e_1^{g/h}))^{q/p} \\ &= \upsilon(2V\cdot e_1^{p/q-1} + 2V\cdot\alpha e_1^{g/h+g/h-2})^{q/p} \\ &= \upsilon(2V)^{q/p}\cdot e_1^{1-q/p}\cdot(1 + \alpha e_1^{g/h-1})^{q/p}\end{aligned} \tag{19}$$

Since $1 < p/q < 2$, $g/h > p/q$ and p, q, g, h are all positive and odd numbers:

$$1 - \frac{q}{p} = \frac{p-q}{p} = \frac{2k}{p},\ (k{=}1, 2\ \cdots) \tag{20}$$

$$\frac{g}{h} - 1 = \frac{g-h}{h} = \frac{2a}{h},\ (a{=}1, 2\ \cdots) \tag{21}$$

where k and a are positive integers, $2k$ and $2a$ are positive even numbers.

$$\dot{V} = \upsilon(2V)^{q/p}\cdot e_1^{2k/p}\cdot(1 + \alpha e_1^{2a/h})^{q/p} \le 0 \tag{22}$$

According to the Lyapunov stability theorem, the origin is in a globally stable state, and the state errors e_1 and e_2 can converge to 0 in finite time according to the sliding mode equivalent condition. The next step is to prove that the improved Super-Twisting control law converges stably on the sliding mode surface.

Proof 2: Selecting the quadratic type positive definite Lyapunov function:

$$\begin{aligned} V_1(x) &= 2k_3|s| + \frac{1}{2}g^2 + \frac{1}{2}s^2 \\ &= 2k_3|s| + \frac{1}{2}g^2 + \frac{1}{2}\left(-k_1|s|^{\frac{1}{2}}sgn(s) + k_2 s + g\right)^2 \end{aligned} \tag{23}$$

Eq. 23 can be expressed as:

$$V_1 = \boldsymbol{\zeta}^{\mathrm{T}}\boldsymbol{Q}\boldsymbol{\zeta} \tag{24}$$

where

$$\boldsymbol{Q} = \frac{1}{2}\begin{bmatrix} (4k_3 + k_1^2) & -k_1k_2 & -k_1 \\ -k_1k_2 & k_2^2 & k_2 \\ -k_1 & k_2 & 2 \end{bmatrix}; \boldsymbol{\zeta} = \begin{bmatrix} |s|^{\frac{1}{2}}\,\mathrm{sgn}(s) \\ s \\ g \end{bmatrix}.$$

Since $k_1 > 0, k_2 < 0, k_3 > 0$, then V_1 is a positive definite and continuous function.

Except for the set $s_1 = \{(x_1, x_2) \in R^2 \mid x = 0\}$, V_1 is differentiable everywhere. When the state error does not converge to 0, the system state cannot be maintained at $s_1 = 0$, so the Chain Rule $d|x|/dt = \dot{x}\mathrm{sgn}(x)$ is applied to calculate $\dot{V}_1$.

Take the derivative of $\boldsymbol{\zeta}$:

$$\begin{aligned} \dot{\boldsymbol{\zeta}} &= \left[|s|^{1/2}\mathrm{sgn}(s)\ s\ g\right]^{\mathrm{T}} \\ &= \frac{1}{|s|^{1/2}}\left[\boldsymbol{W}\boldsymbol{\zeta} + L\zeta + \boldsymbol{\upsilon}\right] \end{aligned} \tag{25}$$

where

$$\boldsymbol{W} = \frac{1}{2}\begin{bmatrix} -k_1 & k_2 & 1 \\ 0 & 0 & 0 \\ -2k_3 & 0 & 0 \end{bmatrix}; \boldsymbol{L} = \begin{bmatrix} 0 & 0 & 0 \\ -k_1 & k_2 & 1 \\ 0 & 0 & 0 \end{bmatrix}; \boldsymbol{\upsilon}^{\mathrm{T}} = \begin{bmatrix} 0 \\ 0 \\ \dot{F} \end{bmatrix}.$$

The derivative of V_1 is:

$$\begin{aligned} \dot{V}_1 &= \dot{\boldsymbol{\zeta}}^{\mathrm{T}}\boldsymbol{Q}\boldsymbol{\zeta} + \boldsymbol{\zeta}^{\mathrm{T}}\boldsymbol{Q}\dot{\boldsymbol{\zeta}} \\ &= -\frac{1}{|s|^{1/2}}\boldsymbol{\zeta}^{\mathrm{T}}\boldsymbol{P}_1\boldsymbol{\zeta} - \boldsymbol{\zeta}^{\mathrm{T}}\boldsymbol{P}_2\boldsymbol{\zeta} + \dot{F}\boldsymbol{\rho}^{\mathrm{T}}\boldsymbol{\zeta} \end{aligned} \tag{26}$$

where

$$P_1 = \frac{1}{2}\begin{bmatrix} 2k_1k_3 + k_1^3 & (k_1^2 + k_3)k_2 & k_1^2 \\ (k_1^2 + k_3)\xi & -k_1k_2^2 & -k_1k_2 \\ k_1^2 & -k_1k_2 & -k_1 \end{bmatrix};$$

$$\boldsymbol{\rho} = \begin{bmatrix} -k_1 \\ k_2 \\ 2 \end{bmatrix}^{\mathrm{T}}; P_2 = k_2\begin{bmatrix} k_1^2 & -k_1k_2 & -k_1 \\ -k_1k_2 & k_2^2 & k_2 \\ -k_1 & k_2 & 1 \end{bmatrix}.$$

According to the limit of Eq. (17):

$$\dot{\boldsymbol{F}}\rho^{\mathrm{T}}\boldsymbol{\zeta} = \frac{1}{|s|^{1/2}}\boldsymbol{\zeta}^{\mathrm{T}}\boldsymbol{M}\boldsymbol{\zeta} \tag{27}$$

where

$$\boldsymbol{M} = \begin{bmatrix} -k_1\dot{F} & 0 & \dot{F} \\ 0 & k_2\dot{F} & 0 \\ \dot{F} & 0 & 0 \end{bmatrix}.$$

Substituting Eq. (27) into Eq. (26):

$$\begin{aligned} \dot{V}_1 &= -\frac{1}{|s|^{1/2}}\boldsymbol{\zeta}^{\mathrm{T}}\boldsymbol{P}_1\boldsymbol{\zeta} - \boldsymbol{\zeta}^{\mathrm{T}}\boldsymbol{P}_2\boldsymbol{\zeta} + \frac{1}{|s|^{1/2}}\boldsymbol{\zeta}^{\mathrm{T}}\boldsymbol{M}\boldsymbol{\zeta} \\ &= -\frac{1}{|s|^{1/2}}\boldsymbol{\zeta}^{\mathrm{T}}(\boldsymbol{P}_1 - \boldsymbol{M})\boldsymbol{\zeta} - \boldsymbol{\zeta}^{\mathrm{T}}\boldsymbol{P}_2\boldsymbol{\zeta} \end{aligned} \tag{28}$$

According to Eq. (28), if $\boldsymbol{P}_1 - \boldsymbol{M} > 0$ and $\boldsymbol{P}_2 > 0$, $\dot{V}_1 < 0$ can be obtained. The necessary and sufficient conditions for $\boldsymbol{P}_1 - \boldsymbol{M} > 0$ are as follows:

$$\begin{cases} k_1^2 + 2k_3 + 2\dot{F}\mathrm{sgn}(s) > 0 \\ 5k_2^2(k_1^2 + 2k_3 + 2\dot{F}\mathrm{sgn}(s)) > 0 \\ k_2^2(9k_1^2 + 8k_3 + 28\dot{F}\mathrm{sgn}(s) + 20\dot{F}^2/k_1^2) < 0 \end{cases} \tag{29}$$

Similarly, the necessary and sufficient conditions of $\boldsymbol{P}_2 > 0$ for:

$$2k_1^2 + k_3 + \dot{F}\mathrm{sgn}(s) > 0 \tag{30}$$

From Eq. (24):

$$\lambda_{\min}(\boldsymbol{Q})\|\boldsymbol{\zeta}\|^2 < V_1 < \lambda_{\max}(\boldsymbol{Q})\|\boldsymbol{\zeta}\|^2 \tag{31}$$

The standard inequality of the quadratic type shows that:

$$|s|^{1/2} \le \|\boldsymbol{\zeta}\| \le V_1^{1/2}/\lambda_{\min}^{1/2}(\boldsymbol{Q}) \tag{32}$$

where $\|\boldsymbol{\zeta}\| = \sqrt{|s| + |s|^2 + |g|^2}$.

From Eq. (32):

$$\begin{aligned} \dot{V}_1 &= -\frac{1}{|s|^{1/2}}\boldsymbol{\zeta}^{\mathrm{T}}(\mathbf{P}_1 - \boldsymbol{M})\boldsymbol{\zeta} - \boldsymbol{\zeta}^{\mathrm{T}}\mathbf{P}_2\boldsymbol{\zeta} \\ &\le -\mu_1 V_1^{1/2} - \mu_2 V_1^{1/2} \\ &\le -\mu_1 V_1^{1/2} \\ &\le 0 \end{aligned} \tag{33}$$

where $\lambda_{\min}(\boldsymbol{Q})$ is the minimum eigenvalue of $\boldsymbol{Q}$;$\lambda_{\max}(\boldsymbol{Q})$ is the maximum eigenvalue of $\boldsymbol{Q}$; $\mu_2 = \lambda_{\min}^{1/2}(\boldsymbol{P}_2)/\lambda_{\max}(\boldsymbol{Q})$; $\mu_1 = \left[\lambda_{\min}^{1/2}(\boldsymbol{Q})\,\delta(\mathbf{P}_1 - \boldsymbol{M})\right]/\lambda_{\max}^{1/2}(\boldsymbol{Q})$.

It can be seen from Eq. (33) that the state error e will converge in finite time.

When the sliding mode surface converges in finite time, that is $s = \dot{s} = 0$, the equivalent control law can be obtained as:

$$u_{eq} = \frac{q}{\beta p}e_2^{2-p/q} \cdot \left(1 + \frac{\alpha g}{h}e_1^{g/h-1}\right) \tag{34}$$

The control law of Eq. (12) is designed by using the improved Super Twisting algorithm as u_{st} follows:

$$u_{st} = k_1|s|^{1/2}\mathrm{sgn}(s) - k_2 s + \int (k_3\mathrm{sgn}(s) + \dot{F})dt \tag{35}$$

According to Eq. (34) and Eq. (35)

$$u_c = u_{eq} + u_{st} \tag{36}$$

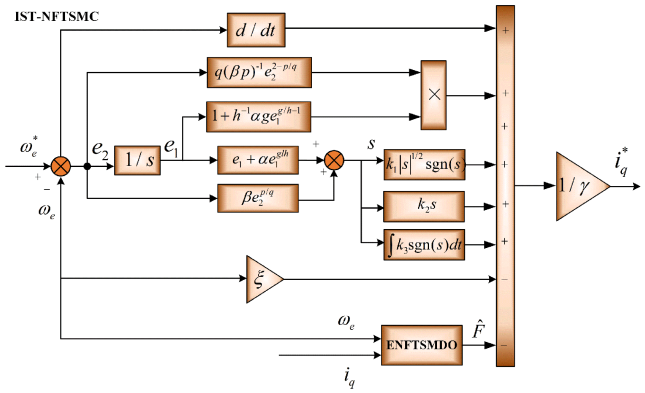

FIGURE 1. The block diagram of IST-NFTSMC speed controller based on ENFTSMDO.

From Eq. (8), (34), (35), and (36), the total control law i_q^* of the speed controller can be obtained:

$$\begin{aligned} i_q^* &= \frac{\dot{\omega}_e^* - \xi\omega_e - \hat{F} + u_{eq} + u_{st}}{\gamma} \\ &= \frac{1}{\gamma}\left[\begin{array}{l} \dot{\omega}_e^* - \xi\omega_e - \tilde{F} + \frac{q}{\beta p} e_2^{2-p/q} \cdot \left(1 + \frac{\alpha g}{h} e_1^{g/h-1}\right) \\ \quad + k_1 |s|^{1/2} \operatorname{sgn}(s) - k_2 s + \int k_3 \operatorname{sgn}(s) dt \end{array}\right] \end{aligned} \tag{37}$$

Figure 1 is the block diagram of the IST-NFTSMC speed controller based on ENFTSMDO.

B. DESIGN OF EXTENDED NFT SLIDING MODE DISTURBANCE OBSERVER

ENFTSMDO can estimate the unknown disturbances part of the system in real-time by measuring the input and output of the actual system, and simultaneously performing feedforward compensation to IST-NFTSMC to improve the anti-interference capability of the system.

Defining variable as follows:

$$x_1 = \hat{\omega}_e - \omega_e \tag{38}$$

Eq. (7) is redefined as:

$$\begin{cases} \dfrac{d\hat{\omega}_e}{dt} = \gamma i_q + \xi\hat{\omega}_e + \hat{F} + u_{smo} \\ \dfrac{d\hat{F}}{dt} = G \cdot u_{smo} \end{cases} \tag{39}$$

where ω'' is the observed speed; F'' is the estimated value of F; $G > 0$; u_{smo} is the control law of sliding mode observer.

From Eq. (7) and Eq. (39) can be obtained:

$$\begin{cases} \dot{x}_1 = \xi x_1 + \tilde{F} + u_{smo} \\ \frac{dF''}{dt} = G \cdot u_{smo} - \ell(t) \end{cases} \tag{40}$$

where F'';$\ell(t) = dF/dt$ is the change rate of disturbances.

Select the state variable as $x_2 = \dot{x}_1 = \dot{\hat{\omega}}_e - \dot{\omega}_e$ and select NFTSM surface [19]:

$$s_1 = x_1 + c_1 x_1^{g_1/t_1} + c_2 x_2^{g_2/t_2} \tag{41}$$

Take the derivative of Eq. (41):

$$\begin{aligned} \dot{s}_1 &= \dot{x}_1 + c_1 \frac{g_1}{t_1} x_1^{g_1/t_1-1} \dot{x}_1 + c_2 \frac{g_2}{t_2} x_2^{g_2/t_2-1} \dot{x}_2 \\ &= \dot{x}_1 + c_1 \frac{g_1}{t_1} x_1^{g_1/t_1-1} \dot{x}_1 + c_2 \frac{g_2}{t_2} x_2^{g_2/t_2-1} \ddot{x}_1 \end{aligned} \tag{42}$$

Design the fast double power reaching law as [28]:

$$\dot{s}_1 = -\tau_1 |s_1|^a \operatorname{sgn}(s_1) - \tau_2 s_1 \tag{43}$$

where τ_1 and τ_2 are normal numbers to be designed; $a = 1-r$; $0 < r < 1$.

$$\begin{aligned} u_{smo} &= u_{eq} + u_{fn} \\ &= \left[\begin{array}{l} -\xi x_1 \\ -\int_0^t \left(\begin{array}{l} \frac{t_2}{c_2 g_2} \dot{x}_2^{2-g_2/t_2} (1 + c_1 \frac{g_1}{t_1} x_1^{g_1/t_1-1}) \\ \quad + \tau_1 |s_1|^a \operatorname{sgn}(s_1) + \tau_2 s_1 \end{array}\right) d\tau \end{array}\right] \end{aligned} \tag{44}$$

where

$$\begin{aligned} u_{eq} &= -\xi x_1; u_{fn} \\ &= -\int_0^t \left(\begin{array}{l} \frac{t_2}{c_2 g_2} \dot{x}_2^{2-g_2/t_2} (1 + c_1 \frac{g_1}{t_1} x_1^{g_1/t_1-1}) \\ \quad + \tau_1 |s_1|^a \operatorname{sgn}(s_1) + \tau_2 s_1 \end{array}\right) d\tau. \end{aligned}$$

Theorem 2: For the state variable Eq. (38), if choose Eq. (41) as the sliding surface, and reaching law as Eq. (43). When the gain satisfies Eq. (45), the system error x_1 converges to 0 in a finite time.

$$\begin{cases} \tau_2 |s_1| \geq \left|\dot{\tilde{F}}\right| \\ \tau_1 |s_1|^a \geq \left|\tilde{F}\right| \end{cases} \tag{45}$$

Proof 3: Select the following Lyapunov function V_1

$$V_1 = \frac{1}{2} s_1^2 \tag{46}$$

Take the derivative of V_1:

$$\begin{aligned} \dot{V}_1 &= s_1 \dot{s}_1 = s_1 \left(\dot{x}_1 + c_1 \frac{g_1}{t_1} x_1^{g_1/t_1-1} \dot{x}_1 + c_2 \frac{g_2}{t_2} x_2^{g_2/t_2-1} \ddot{x}_1\right) \\ &= s_1 \cdot \frac{c_2 g_2}{t_2} \dot{x}_1^{g_2/t_2-1} \\ &\quad \left(\ddot{x}_1 + \frac{t_2}{c_2 g_2} \cdot x_1^{2-g_2/t_2} \cdot \left(1 + \frac{c_1 g_1}{t_1} x_1^{g_1/t_1-1}\right)\right) \end{aligned} \tag{47}$$

Substituting ENFTSMDO control rate Eq. (44) into Eq. (40) yields:

$$\dot{x}_1 = \tilde{F} + u_{fn} \tag{48}$$

Take the derivative of Eq. (48):

$$\ddot{x}_1 = \dot{\tilde{F}} + \dot{u}_{fn} \tag{49}$$

From Eq. (44), Eq. (47) and Eq. (49), it can be obtained:

$$\begin{aligned} \dot{V}_1 &= s_1 \cdot \frac{c_2 g_2}{t_2} \dot{x}_1^{g_2/t_2-1} \left(\dot{\tilde{F}} - \tau_1 |s_1|^a \operatorname{sgn}(s_1) - \tau_2 s_1\right) \\ &= -\frac{c_2 g_2}{t_2} \\ &\quad \dot{x}_1^{g_2/t_2-1} \left(-s_1 \cdot \dot{\tilde{F}} + \tau_1 |s_1|^a \operatorname{sgn}(s_1) \cdot s_1 + \tau_2 s_1 \cdot s_1\right) \\ &= -\frac{c_2 g_2}{t_2} \dot{x}_1^{g_2/t_2-1} \left(-s_1 \cdot \dot{\tilde{F}} + \tau_1 |s_1|^{a+1} + \tau_2 s_1^2\right) \end{aligned} \tag{50}$$

Because of $g_2/t_2 > 0, \dot{x}_1^{g_2/t_2-1} > 0$, Eq. (50) can be converted into two forms:

$$\begin{aligned}\dot{V}_1 &= -\frac{c_2 g_2}{t_2}\dot{x}_1^{g_2/t_2-1}\left(-s_1\cdot\dot{\tilde{F}}+\tau_1|s_1|^{a+1}+\tau_2 s_1^2\right)\\ &\le -\frac{c_2 g_2}{t_2}\dot{x}_1^{g_2/t_2-1}\left(\tau_1|s_1|^{a+1}+|s_1|\left(\tau_2|s_1|-|\dot{\tilde{F}}|\right)\right)\end{aligned} \tag{51}$$

$$\begin{aligned}\dot{V}_1 &= -\frac{c_2 g_2}{t_2}\dot{x}_1^{g_2/t_2-1}\left(-s_1\cdot\dot{\tilde{F}}+\tau_1|s_1|^{a+1}+\tau_2 s_1^2\right)\\ &\le -\frac{c_2 g_2}{t_2}\dot{x}_1^{g_2/t_2-1}\left(\tau_2 s_1^2+|s|\left(\tau_1|s_1|^{a}-|\dot{\tilde{F}}|\right)\right)\end{aligned} \tag{52}$$

If $\left|\dot{\tilde{F}}\right| \le N$ and $N \ge 0$, when $\tau_2|s_1| \ge \left|\dot{\tilde{F}}\right|$, we can get:

$$\begin{aligned}\dot{V}_1 &\le -\frac{c_2 g_2}{t_2}\dot{x}_1^{g_2/t_2-1}\left(\tau_1|s_1|^{a+1}\right)\\ &= -\frac{c_2 g_2}{t_2}\dot{x}_1^{g_2/t_2-1}\left(\tau_1\cdot(2V_1)^{\frac{a+1}{2}}\right)\le 0\end{aligned} \tag{53}$$

When $\tau_1|s_1|^a \ge \left|\dot{\tilde{F}}\right|$:

$$\begin{aligned}\dot{V}_1 &\le -\frac{c_2 g_2}{t_2}\dot{x}_1^{g_2/t_2-1}\left(\tau_2|s_1|^2\right)\\ &= -\frac{c_2 g_2}{t_2}\dot{x}_1^{g_2/t_2-1}\left(\tau_2\cdot 2\,V_1\right)\le 0\end{aligned} \tag{54}$$

According to the Lyapunov stability theorem and comparison lemma [27], it is known that the system will satisfy the sliding mode reachability condition and will converge and remain on the NFTSM surface in a finite time, so that the system error x_1 will converge to 0 in a finite time.

From Eq. (51) and Eq. (52):

$$\begin{cases}|s_1| \le \frac{N}{\tau_2}\\ |s_1| \le \left(\frac{N}{\tau_1}\right)^{\frac{1}{a}}\end{cases} \tag{55}$$

From Eq. (55), the convergence region of the sliding surface s_1 is obtained:

$$|s_1| \le \min\left(\frac{N}{\tau_2}, \left(\frac{N}{\tau_1}\right)^{\frac{1}{a}}\right) \tag{56}$$

From Eq. (43):

$$\begin{aligned}|\dot{s}_1| &\le \tau_1|s_1|^a+\tau_2|s_1|\\ &\le \min\left(\tau_1\cdot\left(\frac{N}{\tau_2}\right)^a, N\right)+\min\left(N, \tau_2\cdot\left(\frac{N}{\tau_1}\right)^{\frac{1}{a}}\right)\end{aligned} \tag{57}$$

Suppose t_r is the convergence time of the sliding surface s_1 from the initial value to the sliding surface $s_1 = 0$. After t_r the system enters the terminal sliding surface and converges to 0 after t_s with a total convergence time of [29]:

$$\begin{aligned}t &= t_r + t_s\\ &= t_r + \int_0^{|x_0|}\frac{c_2^{1/a_2}}{(x+c_1x^{a_1})^{1/a_2}}dx\\ &= \left[t_r + \frac{a_2|x_0|^{1-1/a_2}}{c_1(a_2-1)}\cdot F\left(\frac{1}{a_2}, \frac{a_2-1}{(a_1-1)a_2}; 1+\frac{a_2-1}{(a_1-1)a_2}; -c_1|x_0|^{a_1-1}\right)\right]\end{aligned} \tag{58}$$

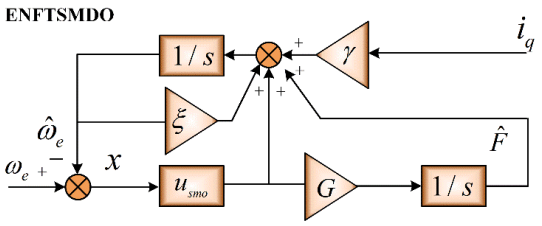

FIGURE 2. The block diagram of ENFTSMDO.

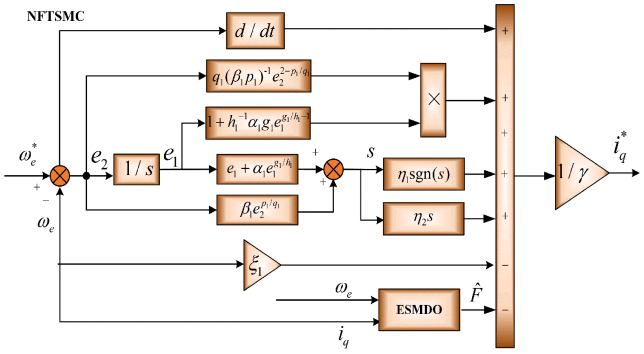

FIGURE 3. The block diagram of NFTSMC speed controller based on ESMDO.

TABLE 1. Nominal parameters of PMSM.

Parameters	Unit	Values
Dc voltage/ u_{dc}	V	600
Rated speed/ n_N	r/min	1900
Stator resistance/ R_s	Ω	2.75
Pole number/ n_p	pairs	2
d axis inductance/ L_d	H	0.004
q axis inductance/ L_q	H	0.009
Magnetic flux/ ψ_f	Wb	0.12
Inertia/ J	$kg\cdot m^2$	0.0029

where $F(\cdot)$ denotes the Gaussian hypergeometric function; $a_1 = g_1/t_1; a_2 = g_2/t_2$.

To reduce the system chattering caused by the sign function, the saturation function $H(s)$ is used instead of the sign function, and the function $H(s)$ is:

$$H(s) = \frac{s}{|s|+\sigma} \tag{59}$$

where $\sigma > 0$; Figure2 is the block diagram of ENFTSMDO.

IV. SIMULATIONS RESULTS

In order to verify the feasibility of the algorithm, MATLAB/Simulink simulation is used to build the IST-NFTSMC algorithm based on ENFTSMDO, which is compared with PI and NFTSMC. IPMSM uses the maximum torque to current ratio (MTPA) control strategy.

Figure 3 is the block diagram of the NFTSMC speed controller based on ESMDO.

TABLE 2. The parameters of the control system.

PI	NFTSMC	IST-NFTSMC
P=105	α_1=0.01	α=0.006
I=15	β_1=0.005	β = 0.03
/	p_1/q_1=7/5	p/q=7/5
/	g_1/h_1=5/3	g/h=5/3
/	η_1 = 0.5	k_1 = 0.1
/	η_2 = 0.005	k_2 = 0.01
/	/	k_3 = 1.55

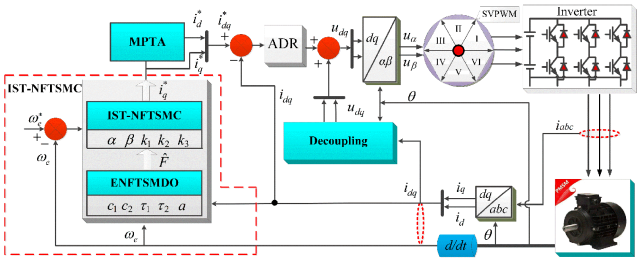

FIGURE 4. The block diagram of the motor speed control system.

The nominal parameters of the motor are shown in Table 1. Table 2 is the control parameters of the three control methods. Figure 4 is the block diagram of the motor speed control system.

Remark 1: The values of γ and ξ in the algorithm of this paper are rectified by $\gamma = 3n_p^2\psi_{ext}/2J$ and $\xi = -B/J$. PI parameter adjustment: First, the current loop transfer function is corrected to a typical type I system, and the P and I of the PI controller are determined according to the dynamic performance index; Then, the current loop is then equated to the speed loop, and the speed loop PI parameters are calibrated to a typical type II system. The gain of the speed loop PI controller is obtained by further fine-tuning according to the operating conditions [22]. *In the NFTSMC algorithm, the exponential reaching law is selected as $\dot{s} = -\eta_1 \mathrm{sgn}(s) - \eta_2 s$, and the disturbance observer is ESMDO* [22].

Remark 2: The selection of slipform surface parameters in IST-NFTSMC directly affects the stability of the motor control system. After selecting α and β approximate parameters to confirm system stability, fine tuning is performed.αbecomes larger, causing the system to overshoot during transients, and the current and torque are also affected. α becomes smaller, causing a slower speed response and a longer time to reach the given value. Contrary to α, a larger β will result in a slower speed response, while a smaller β will result in system oscillation

and motor control performance cannot be guaranteed. The selection of the superhelix control law parameter affects the arrival time of the slipform surface. The selection of the IST-control law parameter affects the arrival time of the slipform surface. Compared with the traditional exponential convergence law, k_2 and k_3 will speed up the speed dynamic response and reach the given speed earlier, but too much will make the speed in the transient steady-state process of serious jitter, current and torque waveform distortion; and a small gain will cause the speed response time to become longer, and the dynamic response speed is affected. Adjusting k_1 at this point can improve this problem by speeding up convergence while reducing jitter.

TABLE 3. Parameter perturbation experimental conditions.

Time/s	Perturbations	Range of Perturbations
1.0	ψ_f /Wb	0.12→0.09
1.5	R_s /Ω	2.75→3.85
2.5	L_q /H	0.009→0.006
3.0	L_d /H	0.004→0.003
3.5	J	0.029→0.04
4.0	B	0.001→0.004
4.5	T_L / N · m	15→ 15 + 2 sin 300t
5.0	T_L / N · m	15 + 2 sin 300t →15
5.5	T_L / N · m	15→20

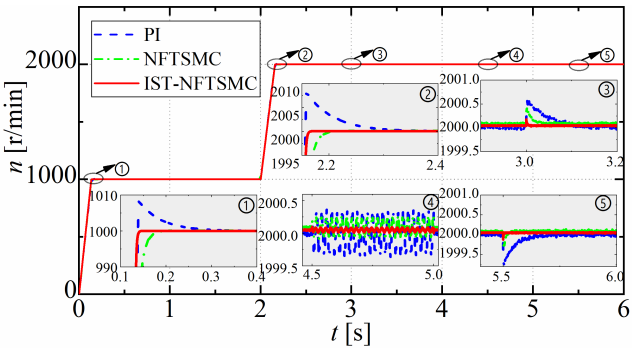

FIGURE 5. Simulation comparison of speed.

Setting the motor inductance, resistance, moment of inertia, viscous friction coefficient and magnet flux parameters to perturb. The anti-interference performance of IST NFTSMC is tested by simulation comparison of PI/NFTSMC/IST NFTSMC with parameter perturbations. The initial speed is 1000r/min and subsequently increases to 2000r/min at 2.0 s. Table 3 represents parameter perturbation experimental conditions.

The following diagrams demonstrate the simulation comparison results of PI, NFTSMC, and IST-NFTSMC. Figure 5 demonstrates the speed response curve; Figure 6 demonstrates the output torque curve; Figure 7(a) shows the current response curve of the *d-axis*; Figure 7(b) shows the current response curve of the *q* axis; Figure 8 shows the comparison of the error curve for speed tracking, Figure 9 shows the observation curve of the total disturbances F controlled by ESMDO and ENFTSMDO.

From Figure 5, when the given speed changes from 0r/min to 1000r/min, the speed controlled by IST-NFTSMC reaches

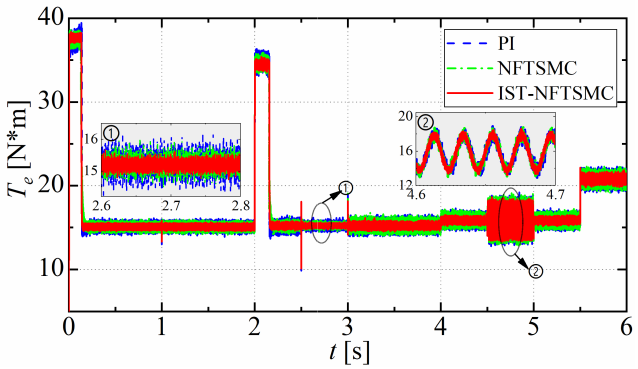

FIGURE 6. Simulation comparison of torque.

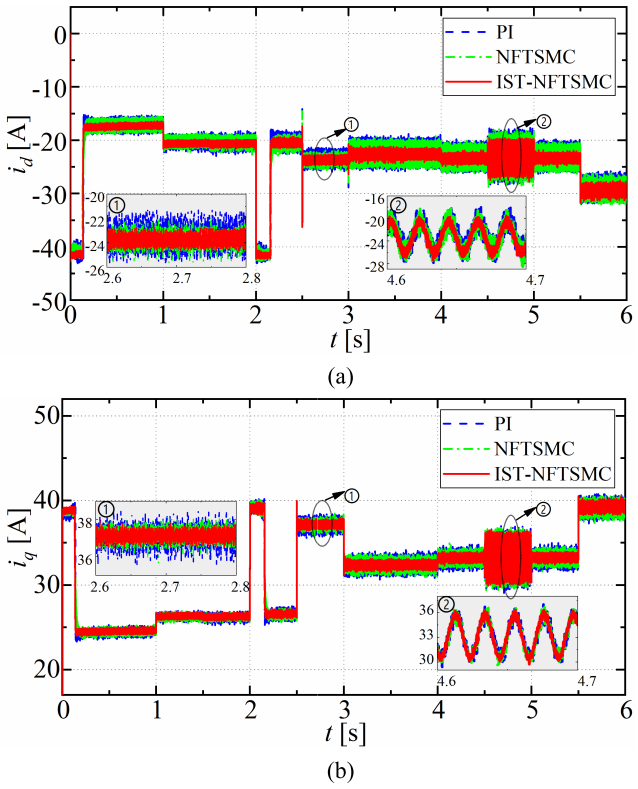

FIGURE 7. Simulation comparison of $d-q$ current. (a) is the d-current. (b) is the q-current.

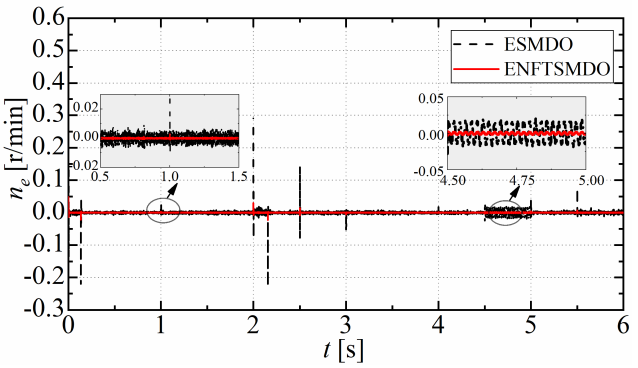

FIGURE 8. Speed tracking error n_e.

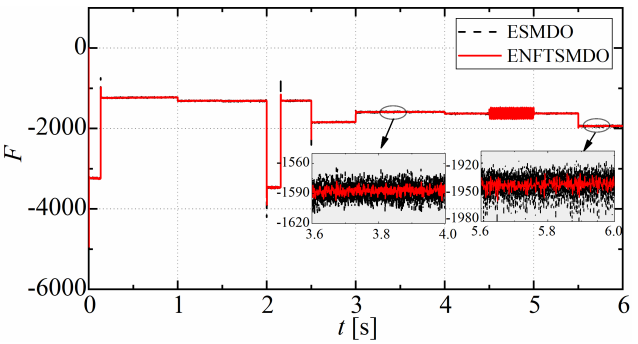

FIGURE 9. The observed value of unknown part F.

the reference speed in 0.12s, and the speed controlled by PI and NFTSMC reaches the steady state in 0.35s and 0.20s respectively. When the given speed changes from 1000r/min to 2000r/min in 2s, the speed controlled by IST-NFTSMC reaches the reference speed in 2.1s, and the speed controlled by PI and NFTSMC reaches the steady state in 2.4s and 2.25s respectively. In summary, in variable speed conditions, IST-NFTSMC has the advantage of no overshoot compared to conventional PI and NFTSMC algorithms, Because of the third-order Super-Twisting control law, which allows the motor speed to reach a given speed quickly. Improving the observation accuracy of perturbation observers for system perturbations by employing the NFTSM surface with the fast double power reaching law, When the parameters of resistance, inductance, magnet flux, the moment of inertia and viscous friction coefficient are perturbed, the speed controlled by PI and NFTSMC can recover to the given speed in a certain time, and have obvious fluctuations and overshoots. while the speed controlled by IST-NFTSMC can accurately track the given speed in a very short time. When the 4.5s system is added with time-varying load torque change, the speed fluctuation range of IST-NFTSMC is small, and the control accuracy is obviously better than PI and NFTSMC. The experimental results show that IST-NFTSMC has strong immunity to scrambling.

Figure 6 and Figure 7 demonstrate that the torque and d-q axis current waveforms of IST-NFTSMC are more stable and have better control performance in both transient and steady states. When the 3.5s B and J are regenerated, the current waveforms of PI and conventional NFTSMC algorithms are distorted and the pulsation increases. when a 4.5s system is added with time-varying load torque variation, the torque ripple and d-q axis current ripple of IST-NFTSMC are minimum.

Figure 8 shows the comparison of the error curve for speed tracking, the ENFTSMDO has better tracking performance. when motor parameters are perturbed, ESMDO has a certain overshoot in the transient process, and the overall tracking error is larger than ENFTSMDO. When the 4.5s system is added with time-varying disturbance, ESMDO has larger buffeting than ENFTSMDO.

Figure 9 shows the observation curve of the total disturbances F controlled by ESMDO and ENFTSMDO. The unknown part of the F waveform observed by ENFTSMDO is smoother, and chattering is effectively reduced. ENFTSMDO effectively enhances the robustness of the system under

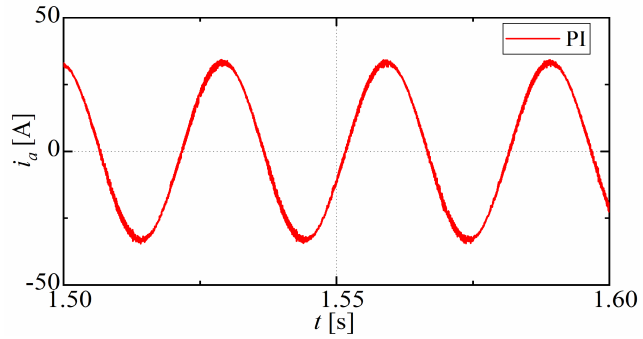

(a)

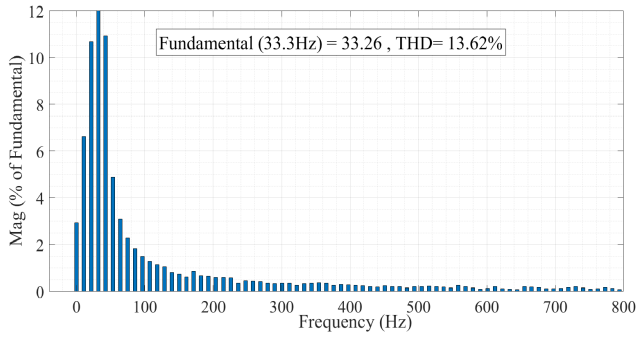

(b)

FIGURE 10. THD analysis of PI's A phase stator current.

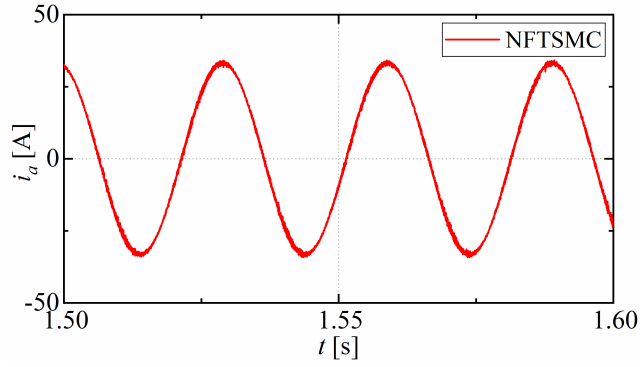

(a)

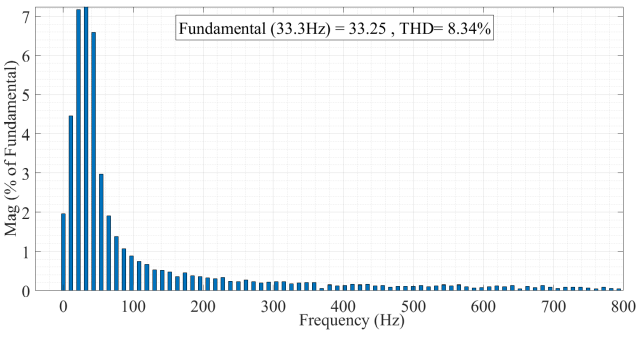

(b)

FIGURE 11. THD analysis of NFTSMC 's A phase stator current.

parameter ingestion by accurately estimating the system F and feeding it back to the IST-NFTSM controller.

Figure 10-12 show the THD analysis diagrams of PI/NFTSMC/IST-NFTSMC's A phase current respectively.

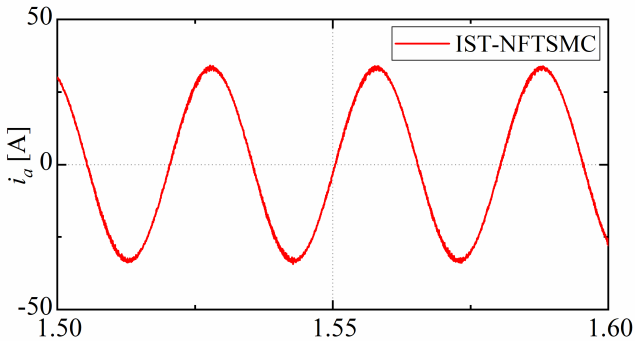

(a)

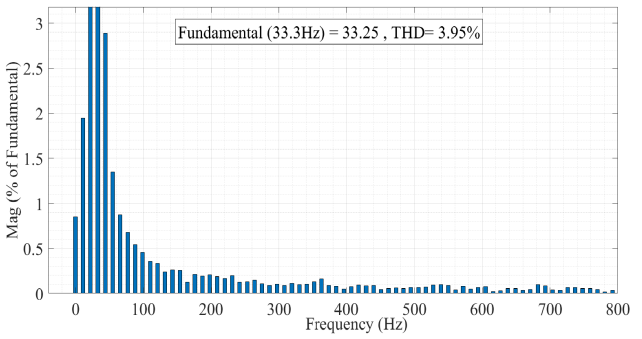

(b)

FIGURE 12. THD analysis of IST-NFTSMC 's A phase stator current.

TABLE 4. Steady state results of speed.

Time/ s	Perturbations	Range of Perturbations	n error r/min
1.0	ψ_f /Wb	0.12→0.09	0.3/0.1/0.05
1.5	R_s /Ω	2.75→3.85	0.08/0.04/0.01
2.5	L_q /H	0.009→0.006	1.3/0.55/0.42
3.0	L_d /H	0.004→0.003	0.6/0.35/0.13
3.5	J	0.029→0.04	0.13/0.08/0.02
4.0	B	0.001→0.004	0.19/0.08/0.02
4.5	T_L / N · m	15→ 15 + 2 sin 300t	0.8/0.35/0.06
5.0	T_L / N · m	15 + 2 sin 300t →15	0.3/0.2/0.03
5.5	T_L / N · m	15→20	0.8/0.45/0.11

From the THD of phase A current in Figure 10-12, the THD of PI, NFTSMC, and IST-NFTSMC are 13.62%, 8.34%, and 3.95% respectively. It can be seen that compared with PI and NFTSMC, the proposed IST-NFTSMC can effectively suppress current harmonics under parameter perturbation. Table 4 is the Steady-state results of speed.

For visual comparison, the speed error comparison datas in Table. 4 is imaged to get Figure 13.

It can be seen that, compared with PI and traditional NFTSMC algorithms, the proposed algorithm accelerates the response speed and improves the control accuracy. The speed controlled by the algorithm proposed in this paper and the NFTSMC algorithm can both recover to the reference value in

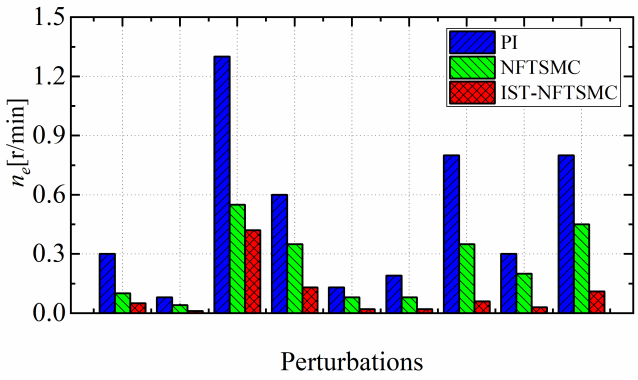

FIGURE 13. Steady state error of speed.

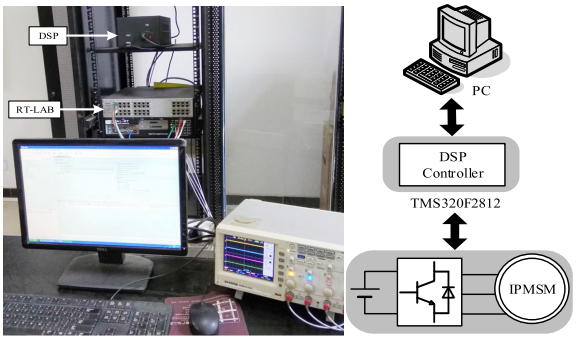

FIGURE 14. RT-LAB experimental platform.

a very short time when the parameters are regenerated. At the same time, the proposed algorithm can reduce the current and torque pulsation amplitude when the IPMSM parameters are ingested, which improves the fast response capability of the system and enhances the overall performance of the IPMSM drive system.

V. RT-LAB EXPERIMENTS RESULTS

Because the electromagnetic parameter perturbation of the motor is difficult to simulate in the actual motor, to further verify the effectiveness of this method, this paper uses RT-Lab to realize the hardware in the loop simulation (HILS) experiment of the IPMSM drive system. Figure 14 is the RT-LAB experimental platform and the motor system is simulated by RT Lab. Figure 15-17 demonstrate the full working condition experiment diagram of PI/NFTSMC/IST-NFTSMC, the experimental parameters are consistent with the simulation parameters.

Figure 15-17 demonstrate the comparison of semi-physical experiment results is consistent with the simulation results. when the motor parameters are perturbed, the overall performance of PI and NFTSMC is affected, and the speed chattering, current, and torque ripple are large. In addition, the current and torque waveforms of PI and NFTSMC are distorted under time-varying disturbances. The Rt-Lab experimental result demonstrates that the IST-NFTSMC control waveform based on ENFTSMDO changes smoothly and can effectively suppress current and torque ripple. Combined with the simulation and semi-physical experiment results, ENFTSMDO observed the disturbance and feedback the controller in the

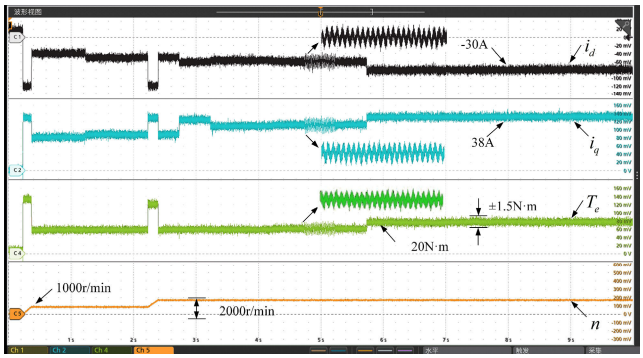

FIGURE 15. The experimental results of PI.

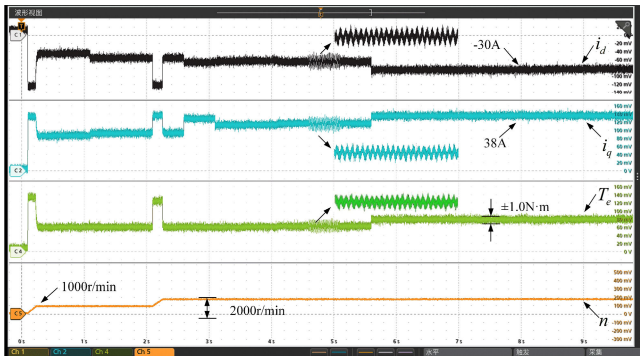

FIGURE 16. The experimental results of NFTSMC.

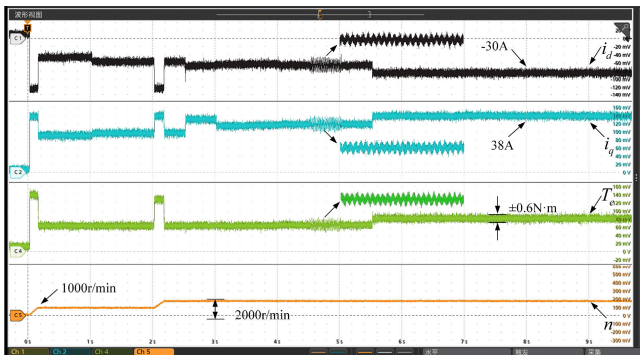

FIGURE 17. The experimental results of IST-NFTSMC.

case of parameter perturbation, effectively speeding up the speed response rate and restraining the current and torque ripple, improving the system's disturbance resistance, and making the motor system have better transient and stable performance.

In conclusion, the IST-NFTSMC control method can effectively suppress the current and torque ripple compared with the traditional PI and NFTSMC in the case of parameter perturbation and unknown disturbance. Table 5 demonstrates the comprehensive control performance comparison of PI, NFTSMC, and IST-NFTSMC control methods.

Remark 3:

1. Speed convergence time: the time to reach the reference speed (s).

2. Speed static difference: amplitude of speed change at steady state (r/min).

TABLE 5. Comparison of PI /NFTSMC /IST-NFTSMC.

Performance indicators	PI	NFTSMC	IST-NFTSMC
Speed convergence time[1]	0.35/0.4	0.2/0.25	0.12/0.1
Torque ripple	18.86%	12.67%	7.34%
Speed static difference[2]	0.1/0.16	0.04/0.09	0.015/0.02
Average speed error rate[3]	0.244	0.117	0.046
i_a THD	13.62%	8.34%	3.95%

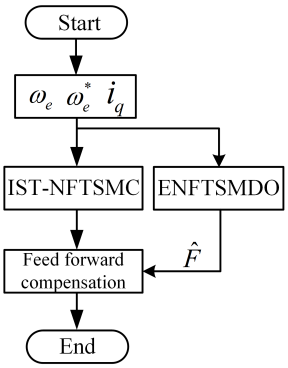

FIGURE 18. Flow chart of IST-NFTSMC.

3. Average speed error rate: the average speed relative error rate with parameter perturbation (%).

The best control performance of the IST-NFTSMC, as can be seen from the data in Table 5. Because the fundamental and harmonic interactions of the air-gap potential in the motor system generate harmonic torque pulsations, ENFTSMDO can accurately observe the disturbance F and provide negative feedback to IST-NFTSMC to effectively reduce torque pulsations and harmonic THD. In addition, the q-axis current pulsation at the output of the speed loop controller is one of the main causes of torque pulsation. Compared with the conventional NFTSMC, the choice of the third-order Super-Twisting control law can effectively reduce the q-axis current pulsation, which serves to reduce torque pulsation and harmonic THD. The specific process is shown in Figure 18:

VI. CONCLUSION

To address the problem that the overall control performance of IPMSM degrades under parameter perturbation and time-varying disturbance, this paper proposes an IST-NFTSMC algorithm for IPMSM based on ENFTSMDO perturbation observer. By comparing the simulation and experiment of PI and NFTSMC under different operating conditions, and analyzing the simulation and experiment results, getting conclusions:

(1) The IST-NFTSMC speed controller based on ENFTSMDO is designed to recover the motor speed, current, and torque to the given values in a very short time under the motor parameter perturbation and unknown disturbance, so that the response speed and robustness of the system can be improved; ENFTSMDO is designed to feed the unknown part of the external disturbance back to the controller for compensation.

(2) Through comprehensive comparison with PI and NFTSMC control algorithms, it is verified that the algorithm still has high precision control performance under different operating conditions such as motor parameters and load time-varying perturbations, which guarantees system reliability and safety while weakening system jitter and enhancing system robustness.

(3) This paper discusses the robust control of IPMSM speed loop, focusing on the study of a new Super-Twisting sliding mode controller for speed loop, which solves the problem of low performance of traditional PI control under parameter ingestion and external disturbance faults. While the current loop PI controller is unable to achieve satisfactory dynamic performance. Therefore, the current-speed double closed loop will be subsequently optimized to improve the robust fault-tolerant control capability of IPMSM against parameter faults including demagnetization and external disturbance faults.

REFERENCES

[1] T. Li and X. Liu, "Model-free non-cascade integral sliding mode control of permanent magnet synchronous motor drive with a fast reaching law," *Symmetry*, vol. 13, no. 9, p. 1680, Sep. 2021.

[2] P. Gao, G. Zhang, and X. Lv, "Model-free hybrid control with intelligent proportional integral and super-twisting sliding mode control of PMSM drives," *Electronics*, vol. 9, no. 9, p. 1427, Sep. 2020.

[3] Y. Zhao, X. Liu, H. Yu, and J. Yu, "Model-free adaptive discrete-time integral terminal sliding mode control for PMSM drive system with disturbance observer," *IET Electr. Power Appl.*, vol. 14, no. 10, pp. 1756–1765, 2020.

[4] M. M. Amin, F. F. M. El-Sousy, O. A. Mohammed, G. A. A. Aziz, and K. Gaber, "MRAS-based super-twisting sliding-mode estimator combined with block control and DTC of six-phase induction motor for ship propulsion application," *IEEE Trans. Ind. Appl.*, vol. 57, no. 6, pp. 6646–6658, Nov. 2021.

[5] C. Y. Xia and U. R. Sadiq, "Inter-turn fault diagnosis of permanent magnet synchronous machine considering model predictive control," *Proc. CSEE*, vol. 40, no. S1, pp. 303–312, 2020, doi: 10.13334/j.0258-8013.pcsee.191394.

[6] Y. Qing, "Application of Kalman filter based on sliding mode PI control in space turntable," *Aerosp. Control*, vol. 39, no. 6, pp. 34–41, 2021.

[7] Z. Bo, Q. Rong, and L. Hui, "Back-stepping sliding mode control of laser cutting permanent magnet linear servo control system," *Trans. China Electrotech. Soc.*, vol. 33, no. 3, pp. 642–651, 2018.

[8] B. Xu, L. Zhang, and W. Ji, "Improved non-singular fast terminal sliding mode control with disturbance observer for PMSM drives," *IEEE Trans. Transp. Electrific.*, vol. 7, no. 4, pp. 2753–2762, Dec. 2021.

[9] J. Cao, X. Sun, and X. Tian, "Optimal control strategy of state feedback control for surface-mounted PMSM drives based on auto-tuning of seeker optimization algorithm," *Int. J. Appl. Electromagn. Mech.*, vol. 66, no. 4, pp. 705–725, Aug. 2021.

[10] M. B. Koura, A. H. Boudinar, A. F. Aimer, A. Bendiabdellah, and Z. Gherabi, "Diagnosis and discernment between eccentricity and demagnetization faults in PMSM drives," *J. Power Electron.*, vol. 21, no. 3, pp. 563–573, Mar. 2021.

[11] K. Zhao, T. Yin, C. Zhang, J. He, X. Li, Y. Chen, R. Zhou, and A. Leng, "Robust model-free nonsingular terminal sliding mode control for PMSM demagnetization fault," *IEEE Access*, vol. 7, pp. 15737–15748, 2019.

[12] R. Li, Z. Wu, and X. Li, "Review on fault diagnosis and active fault tolerant control of permanent magnet synchronous motor drive system," *J. Appl. Sci. Eng.*, vol. 24, no. 2, pp. 185–205, 2021.

[13] G. H. Liu, F. Y. He, and X. Wu, "Flux weakening control of interior permanent magnet synchronous motor based on slide mode controller," *Power Electron.*, vol. 52, no. 3, pp. 82–85, 2018.

[14] K. H. Zhao, C. F. Zhang, J. He, and X. F. Li, "Accurate torque-sensorless control approach for interior permanent-magnet synchronous machine based on cascaded sliding mode observer," *J. Eng.*, vol. 2017, no. 7, pp. 376–384, 2017.
[15] W. Liu, S. Chen, and H. Huang, "Adaptive nonsingular fast terminal sliding mode control for permanent magnet synchronous motor based on disturbance observer," *IEEE Access*, vol. 7, pp. 153791–153798, 2019, doi: 10.1109/access.2019.2948945.
[16] P. T. H. Sen, N. Q. Minh, D. T. T. Anh, D. T. T. Anh, and P. X. Minh, "A new tracking control algorithm for a wheeled mobile robot based on backstepping and hierarchical sliding mode techniques," in *Proc. 1st Int. Symp. Instrum., Control, Artif. Intell., Robot. (ICA-SYMP)*, Jan. 2019, pp. 25–28, doi: 10.1109/ICA-SYMP.2019.8646288.
[17] L. Yuan and J. Li, "Consensus of discrete-time nonlinear multiagent systems using sliding mode control based on optimal control," *IEEE Access*, vol. 10, pp. 47275–47283, 2022, doi: 10.1109/ACCESS.2022.3171825.
[18] A. K. Junejo, W. Xu, C. Mu, M. M. Ismail, and Y. Liu, "Adaptive speed control of PMSM drive system based a new sliding-mode reaching law," *IEEE Trans. Power Electron.*, vol. 35, no. 11, pp. 12110–12121, Nov. 2020, doi: 10.1109/TPEL.2020.2986893.
[19] X. Zhou, W. Wang, Z. Liu, C. Liang, and C. Lai, "Impact angle constrained three-dimensional integrated guidance and control based on fractional integral terminal sliding mode control," *IEEE Access*, vol. 7, pp. 126857–126870, 2019.
[20] Z. Kaihui, Z. Ruizhui, L. Aojie, D. Wangke, and H. Gang, "Finite control set model-free fault-tolerant predictive control for permanent magnet synchronous motor," *Trans. China Electrotech. Soc.*, vol. 36, no. 1, pp. 27–38, 2021.
[21] M. Yunkui, L. Xiangfei, and C. Xuan, "Permanent magnet flux linkage observation of adaptive high-order sliding mode permanent magnet synchronous motor," *J. Electron. Meas. Instrum.*, vol. 34, no. 3, pp. 163–170, 2020.
[22] Z. Kaihui, "Research on model-free sliding mode control of permanent magnet synchronous motor," *J. Electron. Meas. Instrum.*, vol. 32, no. 4, pp. 172–180, 2018.
[23] K. H. Zhao, W. K. Dai, and R. R. Zhou, "Novel model-free sliding mode control of permanent magnet synchronous motor based on extended sliding mode disturbance observer," *Proc. CSEE*, vol. 42, no. 6, pp. 2375–2386, 2022.
[24] L. Hou, J. Ma, and W. Wang, "Sliding mode predictive current control of permanent magnet synchronous motor with cascaded variable rate sliding mode speed controller," *IEEE Access*, vol. 10, pp. 33992–34002, 2022, doi: 10.1109/ACCESS.2022.3161629.
[25] H. Benbouhenni, "Intelligent super twisting high order sliding mode controller of dual-rotor wind power systems with direct attack based on doubly-fed induction generators," *J. Elect. Eng., Electron., Control Comput. Sci.*, vol. 7, no. 4, pp. 1–8, 2021.
[26] F. P. Scalcon, G. Fang, R. P. Vieira, H. A. Grundling, and A. Emadi, "Discrete-time super-twisting sliding mode current controller with fixed switching frequency for switched reluctance motors," *IEEE Trans. Power Electron.*, vol. 37, no. 3, pp. 3321–3333, Mar. 2022.
[27] L. Qu, W. Qiao, and L. Qu, "An extended-state-observer-based sliding-mode speed control for permanent-magnet synchronous motors," *IEEE J. Emerg. Sel. Topics Power Electron.*, vol. 9, no. 2, pp. 1605–1613, Apr. 2021.
[28] Z. Hu, H. Gao, H. Du, and M. Fan, "Research on SVM-DTC control strategy of PMSM based on super-twisting sliding mode active disturbance rejection control," in *Proc. IEEE 5th Int. Electr. Energy Conf. (CIEEC)*, May 2022, pp. 636–640, doi: 10.1109/CIEEC54735.2022.9846588.
[29] H. Yishan, T. Runzhong, K. Mingqiu, L. Jianhua, Z. Kaihui, and C. Xiang, "Improved modelless sliding mode control of permanent magnet synchronous motor drive system based on fast approaching law," *Locomotive Electr. Transmiss.*, vol. 286, no. 3, pp. 148–155, 2022, doi: 10.13890/j.issn.1000-128X.2022.03.019.
[30] S. F. Xiong, W. H. Wang, and S. Wang, "Nonsingular fast terminal sliding-mode guidance with intercept angle constraint," *Control Theory Appl.*, vol. 31, no. 3, pp. 269–278, 2014.

XIANGFEI LI received the M.S. degree from Zhengzhou University, Zhengzhou, China, in 1999, and the Ph.D. degree in control theory and control engineering from Central South University, Changsha, China, in 2003. He is currently a Professor with the College of Electrical and Information Engineering, Hunan University of Technology, Zhuzhou. His current research interests include electric traction and transmission control.

JUNQIN LIU received B.Sc. degree from the Changsha University of Science & Technology, in 2021. He is currently pursuing the M.S. degree with the College of Electrical and Information Engineering, Hunan University of Technology, Zhuzhou, China.

His research interests include electric drive technology and its fault diagnosis.

YANG YIN received the B.Sc. degree from the Hunan University of Technology, in 2020, where he is currently pursuing the M.Sc. degree. His research interests include electric drive technology and its fault diagnosis.

KAIHUI ZHAO (Senior Member, IEEE) received the B.S. degree in electric traction and transmission control from the Changsha Railway Institute, Changsha, China, in 1997, the M.S. degree in computer application technology from Southeast University, Nanjing, China, in 2005, and the Ph.D. degree in traffic information engineering and control from Central South University, Changsha, in 2015.

Since 2005, he has been with the College of Electrical and Information Engineering, Hunan University of Technology, Zhuzhou, where he has been an Associate Professor, since 2007. His research interests include intelligent control and fault diagnosis of permanent magnet synchronous motor.